



Fluorescence imaging enabled poly(lactide-co-glycolide)



Jianqing Hu ^{a,b}, Jinshan Guo ^b, Zhiwei Xie ^b, Dingying Shan ^b, Ethan Gerhard ^b, Guoying Qian ^c, Jian Yang ^{b,*}

^a School of Chemistry and Chemical Engineering, South China University of Technology, Guangzhou 510640, China

^b Department of Biomedical Engineering, Materials Research Institute, The Huck Institutes of The Life Sciences, The Pennsylvania State University, University Park, PA 16802, USA

^c Zhejiang Provincial Top Key Discipline of Bioengineering, College of Biological and Environmental Sciences, Zhejiang Wanli University, Ningbo 315100, China

ARTICLE INFO

Article history:

Received 25 August 2015

Received in revised form 28 September 2015

Accepted 9 October 2015

Available online 20 October 2015

Keywords:

Biodegradable

Photoluminescence

Bioimaging

Tissue engineering

Drug delivery

PLGA

ABSTRACT

Fluorescent biomaterials have attracted significant research efforts in the past decades. Herein, we report a new series of biodegradable, fluorescence imaging-enabled copolymers, biodegradable photoluminescent poly(lactide-co-glycolide) (BPLP-co-PLGA). Photoluminescence characterization shows that BPLP-co-PLGA solutions, films and nanoparticles all exhibit strong, tunable and stable photoluminescence. By adjusting the molar ratios of L-lactide (LA)/glycolide (GA) and (LA + GA)/BPLP, full degradation of BPLP-co-PLGA can be achieved in 8–16 weeks. The fluorescence decay behavior of BPLP-co-PLGA can be used for non-invasive monitoring of material degradation. In vitro cytotoxicity and in vivo foreign body response evaluations demonstrate that BPLP-co-PLGA exhibits similar biocompatibility to poly(lactide-co-glycolide) (PLGA). The imaging-enabled BPLP-co-PLGA was fabricated into porous scaffolds whose degradation can be monitored through non-invasive imaging and nanoparticles that show therapeutic potential demonstrated by fluorescent cellular labeling, imaging and sustained 5-fluorouracil delivery. The development of inherently fluorescent PLGA copolymers is expected to impact the use of already widely accepted PLGA polymers for applications where fluorescent properties are highly desired but limited by the conventional use of cytotoxic quantum dots and photobleaching organic dyes.

Statement of significance

This manuscript describes a novel strategy of conferring intrinsic photoluminescence to the widely used biodegradable polymers, poly(lactide-co-glycolide) without introducing any cytotoxic quantum dots or photo-bleaching organic dyes, which may greatly expand the applications of these polymers in where fluorescent properties are highly desired. Given the already significant impact generated by the use of PLGA and alike, this work contributes to fluorescence chemistry and new functional biomaterial design and will potentially generate significant impact on many fields of applications such as tissue engineering, molecular imaging and labeling, and drug delivery.

© 2015 Acta Materialia Inc. Published by Elsevier Ltd. All rights reserved.

1. Introduction

Emerging biomedical technologies rely on the development of advanced biomaterials, including the development of medical materials with improved functionality and the application of these biomaterials to new fields [1–3]. During the past decades, as emergent biomaterials, biodegradable polymers have received extensive research and development efforts for biomedical applications, such as tissue engineering, regenerative medicine and drug delivery [4–8]. Recently, the development of biodegradable polymers with

imaging capabilities, especially fluorescence imaging, to analyze biomolecules, track biological processes, and visualize diseases and therapeutic efficacy, has become increasingly desirable [9,10]. In particular, non-invasive evaluation of biodegradable materials, real-time monitoring of tissue engineering scaffolds and targeted drug delivery are emerging fields that demand biodegradable photoluminescent polymers. To date, tremendous effort has been made to mix or conjugate biodegradable polymers with semiconducting quantum dots or organic dyes to create photoluminescent biodegradable materials [11–14]. However, the inevitable photobleaching and low dye-to-polymer labeling ratios of organic dyes and the innate toxicity from the heavy metal of quantum dots prevent their practical use in vivo [15,16]. Green

* Corresponding author at: W340 Millennium Science Complex, University Park, PA 16802, USA.

E-mail address: jxy30@psu.edu (J. Yang).

fluorescent protein (GFP) is an alternative that shows intrinsic photoluminescence, but it is still capable of causing cellular toxicity due to over-expression and protein aggregation. There are also few reports on combining GFP with biodegradable polymers [17,18]. Thus, the development of biocompatible and highly photo-stable biodegradable, photoluminescent polymers for imaging-aided tissue engineering and drug delivery still remains a significant challenge.

Recently, our lab has made a progress in the development of biodegradable photoluminescent polymer (BPLP) with inherent photoluminescence. BPLPs have tunable fluorescence with high quantum yields (up to 62.33%) and superior photo-stability, making BPLPs promising materials for a wide range of biomedical applications [19]. BPLP is a fully degradable and cyto-compatible aliphatic oligomer with low-molecular weight (\sim 1200 Da) which can be thermally crosslinked into biodegradable elastomers. However, the tensile strength of crosslinked BPLP is not high enough for many tissue engineering applications. In addition, BPLP nanoparticles tend to aggregate in physiological conditions due to their sticky nature, caused by its low molecular weight, which limits the application of BPLP nanoparticles as theranostic probes [20]. A practical approach to address the above issues is to incorporate BPLP into traditional or commercialized biodegradable polymers to achieve higher molecular weight, improved mechanical strength, and favorable processability. Our efforts have led to the development of urethane-doped BPLP (UBPLP) and BPLP-co-poly(ϵ -lactide) (BPLP-PLLA) [20,21]. However, the synthesis of BPLP-PLLA used an enzyme-catalyzed polymerization process, which cannot be applied in large-scale industrial production. Additionally, the application of PLLA polymers is limited by their rigidity, brittleness and slow degradation. To expand the application of these fluorescent polymers in soft tissue engineering and drug delivery and explore the possibility of their large-scale industrial production, we incorporated BPLP into the relatively fast-biodegradable polymers, poly(lactide-co-glycolide) (PLGA), using an industrially used coordination polymerization process. PLGA has been widely accepted as the gold standard material for many drug delivery and tissue engineering devices approved by the U.S. Food and Drug Administration (FDA) due to its favorable biocompatibility, relatively fast biodegradation rate, and considerable mechanical strength [22–26]. PLGA can be conveniently synthesized through a ring-opening polymerization of cyclic dimers of lactic acid and glycolic acid, lactide (LA) and glycolide (GA), initiated by hydroxyl group-containing compounds [27–29]. Varying the molar ratio of LA/GA and monomer/initiator results in tailored mechanical performance and degradation profiles that supporting controlled drug release and tissue regeneration. By controlling the BPLP synthesis procedure, excessive hydroxyl groups, which can initialize PLGA polymerization, remain present at the chain ends of BPLP [19,21,30]. In this study, a new family of biodegradability tunable, inherently photoluminescent BPLP-poly(lactide-co-glycolide) (BPLP-co-PLGA) copolymers were synthesized. Chemical, thermal, mechanical, and optical properties, as well as the degradation and biocompatibility of the resulting BPLP-co-PLGA copolymers have been comprehensively examined. BPLP-co-PLGA copolymers present several remarkable features: (i) inherent photoluminescence inherited from BPLP [19,31]; (ii) excellent biocompatibility; (iii) Tunable thermal and mechanical properties, degradation rates and luminescence by varying compositions of BPLP, LA and GA during copolymer synthesis; and (iv) good processability for the fabrication of films, micro-/nano-particles and porous scaffolds. The strategy of combining BPLP with PLGA to produce inherently photoluminescent PLGA copolymers may open new avenues in numerous biomedical applications for which both biodegradable materials and optical imaging are highly desired.

2. Experimental section

2.1. Synthesis of BPLP-co-PLGA copolymers

BPLP-co-PLGA copolymers were synthesized in two steps (Fig. 1a). Step one involves the synthesis of a hydroxyl-terminated BPLP prepolymer as described in our previous work [19]. Representative citric acid, 1, 8-octanediol and ϵ -cysteine with the molar ratio of 1:1.1:0.2 were added into a three-necked round bottom flask and then heated to 160 °C under a constant flow of nitrogen till all reactants melted. The temperature of the reaction was subsequently lowered to 140 °C and the solution was allowed to react for another \sim 1 h. The reaction was stopped before the stirring bar stopped stirring completely by adding 1,4-dioxane to dissolve the obtained prepolymer. The obtained prepolymer was purified by drop-wise precipitation of prepolymer solution in 1,4-dioxane into deionized water to remove unreacted monomers. The purified prepolymer was collected and lyophilized in a Freeze 6 Freeze Dryer (Labconco, Kansas City, MO) for 24 h to obtain BPLP prepolymer, BPLP-Cys. The fluorophore structure of BPLP-Cys was recently verified as a fused ring structure ((5-oxo-3,5-dihydro-thiazolopyridine-3,7-dicarboxylic acid, TPA) (Fig. 1a) [31].

In the second step, the BPLP prepolymer was used as a macro-initiator to react with ϵ -lactide and glycolide via a ring-opening polymerization catalyzed by stannous 2-ethylhexanoate (Sn (OCT)₂) to obtain BPLP-co-PLGA copolymers. Briefly, ϵ -lactide and glycolide at various molar ratios were added to an oven-dried reaction tube with various amounts of BPLP prepolymers. Then, Sn (OCT)₂ (0.1% by weight of ϵ -lactide and glycolide mixture) was added as a solution in dry dichloromethane. The dichloromethane was evaporated in vacuum over a period of 1 h. The tube was vacuumed and purged with nitrogen three times, and then flame-sealed and subsequently immersed in a 160 °C oil bath for 48 h. After 48 h, the reaction product was cooled to ambient temperature. The obtained solid materials were dissolved in chloroform and precipitated three times in an excess of pure ethanol to remove unreacted raw materials. Finally, BPLP-co-PLGA copolymers were recovered by vacuum filtration and dried in vacuum at room temperature for at least 1 week.

2.2. Fabrication of BPLP-co-PLGA copolymers films, scaffolds and nanoparticles

BPLP-co-PLGA films were prepared by casting their dichloromethane solution into poly(tetrafluoroethylene) (PTFE) dishes followed by evaporation [32]. BPLP-co-PLGA scaffolds were fabricated by a convenient salt-leaching method. BPLP-co-PLGA copolymers were dissolved in 1,4-dioxane, followed by the addition of sieved salt with a desired size. The solvent was evaporated and the salt was leached out by DI water, and the samples were freeze-dried for 24 h to obtain BPLP-co-PLGA scaffolds. BPLP-co-PLGA nanoparticles and 5-fluorouracil (5-Fu) loaded BPLP-co-PLGA nanoparticles were prepared using single emulsion (O/W) method and double emulsion (W/O/W) method, respectively. For BPLP-co-PLGA nanoparticle preparation, 100 mg of the BPLP-co-PLGA copolymers were dissolved in 5 mL of chloroform. The polymeric solution was then added dropwise to 40 mL of the PVA aqueous solution (5%, w/v) and ultrasonicated simultaneously to produce an oil-in-water (O/W) emulsion. The O/W emulsion was stirred for 24 h in a chemical hood to evaporate chloroform. The resultant nanoparticles were collected by centrifugation and washed with distilled water three times followed by freeze-drying to obtain a fine powder of BPLP-co-PLGA nanoparticles. For 5-Fu loaded BPLP-co-PLGA nanoparticle preparation, 100 mg of the BPLP-co-PLGA copolymers

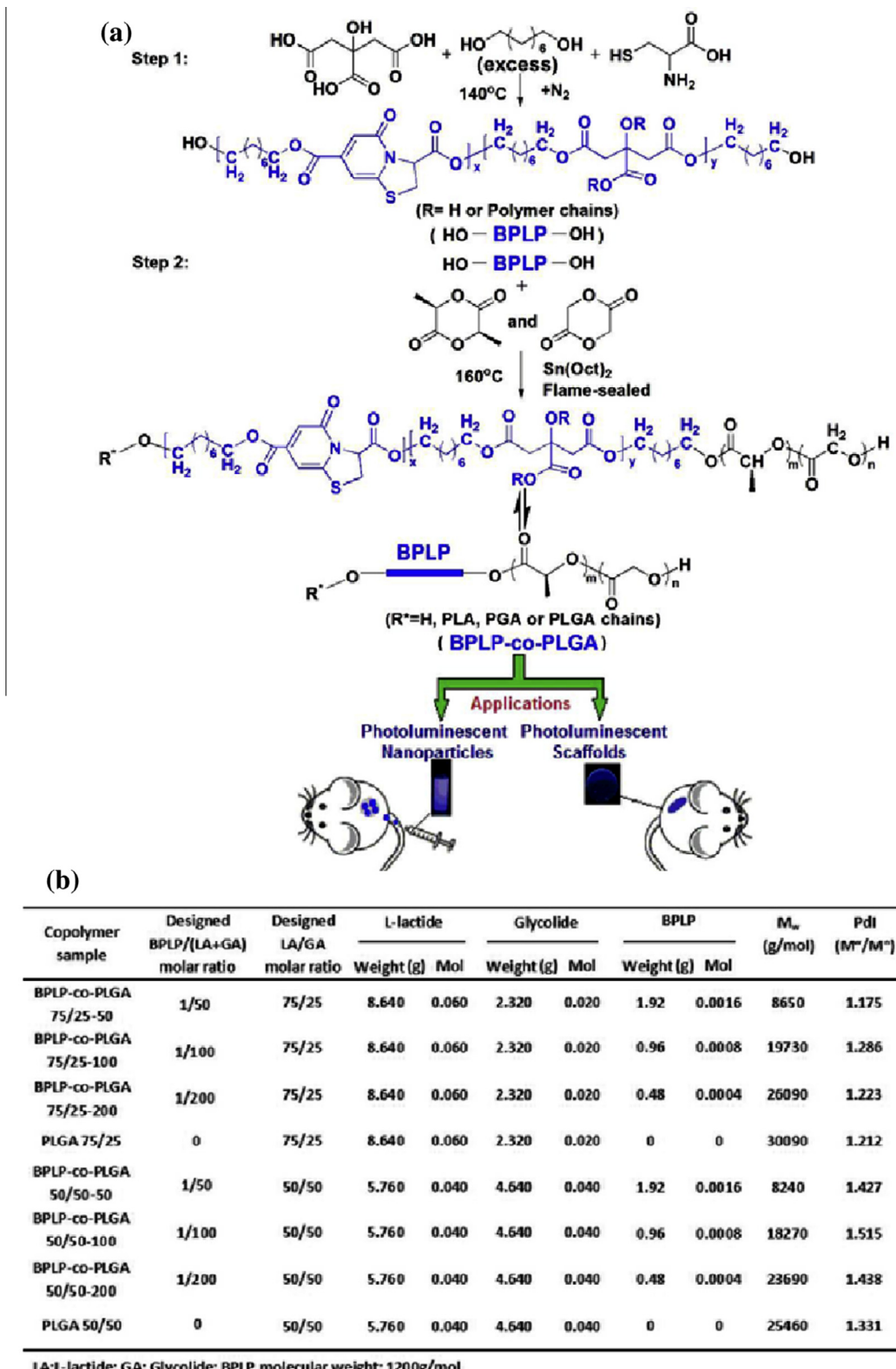


Fig. 1. (a) Synthesis of BPLP-co-PLGA. Step 1: synthesis of BPLP via polycondensation; step 2: synthesis of BPLP-co-PLGA via a ring-opening polymerization using BPLP as a macromolecular initiator. (b) Feeding ratios, molecular weights (M_w), polydispersity indexes (PDI), and intrinsic viscosities ($[\eta]$) of PLGA and BPLP-co-PLGA copolymers synthesized in this study.

were dissolved in 5 mL of chloroform. 2 mL 5-Fu aqueous solution (5 mg/mL) was slowly added into BPLP-co-PLGA organic solution and ultrasonicated simultaneously. The primary water-in-oil (W/O) emulsion was formed and was slowly added into 40 mL of

the PVA aqueous solution (5%, w/v) by ultrasonication homogenization to produce the water-in-oil-in-water (W/O/W) emulsion. The W/O/W emulsion was stirred for 24 h in a chemical hood to evaporate chloroform. The resultant nanoparticles were collected

by centrifugation and washed with deionized (DI) water three times followed by freeze-drying to give the 5-Fu loaded BPLP-co-PLGA nanoparticles.

2.3. Polymer general characterization

Molecular weights and molecular weight distributions of BPLP-co-PLGA and PLGA copolymers were measured using a Shimadzu HPLC system equipped with a Phenomenex Phenogel 5 μm 10E3 SEC column, a Wyatt miniDAWN light scattering detector and an OptiLab RI detector. PLGA and BPLP-co-PLGA copolymers were dissolved in chloroform (chloroform was used as the mobile phase as well). For each experiment, the injection volume was 100 μL, while a flow rate of 1 mL/min and 40 °C column temperature was used. 30 KDa monodisperse polystyrene served as the standard for calibration of both detectors. Intrinsic viscosities of copolymers were also measured following the steps as described below: 50 mg of PLGA or BPLP-co-PLGA copolymer was dissolved in 10 mL chloroform to make a polymer solution, which was then filtered into an Ubbelohde viscometer (size 1, Paragon Scientific Ltd., UK) using a 0.22 μm PTFE syringe filter. The filled viscometer was equilibrated in a 30 °C water bath for 15 min. The flux time of pure chloroform and the polymer solution between two marks was recorded. Three measurements were performed for each sample, and the variation of flux time was limited within 0.3 s. The intrinsic viscosity ($[\eta]$) was calculated using the following Eq. (1):

$$[\eta] = \frac{\sqrt{2(\eta_r - 1 - \ln \eta_r)}}{C} \quad (1)$$

where η_r is the relative viscosity (the flux time ratio of the polymer solution to the pure chloroform) and C is the polymer concentration in units of grams per deciliter.

¹H NMR spectra were obtained in chloroform-d at 300 MHz using a Bruker DPX-300 FT-NMR spectrometer. Attenuated total reflectance-Fourier transform infrared (ATR-FTIR) characterization was performed on a Bruker Vertex 70 FTIR spectrometer with a Pike Miracle Single-Bounce diamond crystal plate accessory at room temperature. FTIR spectra were recorded over a wavelength range of 4000–500 cm⁻¹. Mechanical tests were conducted with an Instron 5966 machine fitted with a 500 N load cell. The copolymer films cut into rectangle shaped specimens were loaded and pulled at a rate of 500 mm min⁻¹, and elongated to failure. The Young's modulus was calculated by measuring the gradient from 0% to 10% elongation of the stress-strain curve. Six specimens per sample were tested and averaged. The thermal properties of copolymers were characterized by differential scanning calorimetry (DSC, -50–150 °C) (TA Instruments Q2000) and thermal gravimetric analysis (TGA, 20–600 °C) (TA instruments 2050 TGA) at a heating rate of 10 °C/min under nitrogen atmosphere. The water-in-air contact angles of copolymer films were measured at room temperature by a Rame-Hart goniometer and imaging system (Rame-Hart Model 295) within 10 s after dropping. Four independent measurements at different sites were averaged. The change of water-in-air contact angle with time was also monitored from 0 to 75 min after water was dropped on the surface of the films. The morphologies of films and scaffolds were observed by scanning electron microscope (SEM) (Hitachi 3500N, EPIC). The morphology of nanoparticles was observed by transmission electron microscopy (TEM, Philips EM 420). The particle size and size distribution of nanoparticles were measured by dynamic light scattering (DLS) (Malvern Zetasizer).

2.4. Photoluminescent properties

All photoluminescence spectra were acquired on HORIBA Scientific Fluoromax-4 spectrofluorometer. All copolymers were

dissolved in chloroform to test photoluminescence unless otherwise noted. Both the excitation and the emission slit widths were set at 1.5 nm. The quantum yields of copolymers were measured by the Williams' method [33]. Anthracene (quantum yield = 27% in ethanol) was used as the standard. The extinction coefficient (ϵ , mol⁻¹ L cm⁻¹) of BPLP-co-PLGA was calculated according to the Beer-Lambert law, $A = \epsilon CL$. Here C and L are the concentration (mol/L) and length (cm) of the dye solution in a UV-vis cuvette respectively. The brightness and photostability are two important intrinsic photophysical properties of fluorescent materials. The brightness intensities of BPLP-co-PLGA can be calculated by the extinction coefficient times the quantum yield. Photostability was measured by continuously illuminating copolymer solutions with excitation light at 365 nm and measuring the resulting emission at 430 nm for 3 h. Photoluminescence stability of rhodamine B was tested with its maximum excitation at 540 nm and maximum emission at 625 nm for the same 3 h in aqueous solution. For nanoparticle photoluminescence characterization, the copolymer nanoparticles were dispersed in DI water and tested using the same method used for copolymer solutions. All the experiments were carried out in triplicate.

2.5. In vitro degradation

In vitro degradation was conducted with 50 mg of copolymer film (with thickness around 0.15–0.30 mm) placed in a tube containing 10 mL of phosphate buffered saline (PBS, pH = 7.4) and incubated at 37 °C. PBS was replaced every two weeks until complete degradation. At each time point, the samples were taken out and thoroughly washed with deionized water 3 times, lyophilized for 1 week, each sample was weighed and the degradation was calculated by mass loss. Six parallel tests were averaged at each time point and the results are presented as means ± standard deviation. The effect of degradation on photoluminescence was also monitored by testing the photoluminescence of degrading copolymers as well as the supernatant PBS.

2.6. In vitro cytotoxicity of copolymer films and degradation products

Cytotoxicity of BPLP-co-PLGA films was quantitatively assessed by Methylthiazoletrazolium (MTT) assay against human mesenchymal stem cells (hMSCs, Lonza Walkersville Inc, US). PLGA 75/25 was used as a control. All testing films were cut into circular discs (7 mm in diameter) to fit the inner diameter of 96-well plates. The films were sterilized in 70% ethanol for 3 h followed by another 30 min exposure to UV light. Subsequently, 200 μL of a cell suspension (5×10^4 cells/mL) in complete Dulbecco's modified eagle's medium (DMEM, with 10% (v/v) fetal bovine serum (FBS) and 1% (v/v) penicillin streptomycin) was added to each well in a 96-well plate with disk-shaped specimens on the bottom. The culture plates were maintained in an incubator at 37 °C, 5% CO₂ and 95% relative humidity. MTT assay analysis was performed after 24 h of culture as per the manufacturer's protocol. Absorbance was analyzed with an Infinite 200 microplate reader (Tecan Group Ltd., Switzerland) at 570 nm. At the same time, the cell morphology of hMSCs on copolymer films after 1 day culture was observed by scanning electron microscopy (SEM) after cell fixing, gradient dehydration by ethanol solutions with increasing concentrations (from 50%, 70%, to 90% and finally 100%), and freeze-drying.

The cytotoxicity of BPLP-co-PLGA degradation products was also evaluated against hMSCs. Equal weight (0.25 g) of PLGA and BPLP-co-PLGA copolymers were fully degraded in 5 mL of 1 M NaOH solution and the resultant solutions were adjusted to pH 7.4 with 0.5 M HCl solution and then were diluted to 1×, 10× and 100× concentrations (1× was the pH adjusted solution of degradation products with no dilution; 10× and 100× means 10

times and 100 times dilution of 1× solution, respectively) using PBS (pH 7.4). All the above solutions were passed through a sterilized 0.22 µm filter prior to use for cell culture. To each well of a 96-well cell culture plate, 200 µL of hMSC cell solution in complete DMEM with a density of 5×10^4 cells/mL was added. On the second day, 20 µL of degradation products with 1×, 10× and 100× concentrations were added and cells were incubated for another 24 h followed by MTT assay analysis. The cell viabilities of hMSCs in media containing polymer degradation solutions were normalized to that of cells cultured in normal media. To assess the effect of polymer degradation products on cell proliferation, Live/Dead staining assay (Life Technologies Inc., US) was conducted on hMSCs cultured in 10× degradation products 1 day, 3 days and 7 days post cell seeding and the addition of 10× degradation products to complete DMEM medium. Cell culture media containing 200 µL of complete DMEM and 20 µL of 10× polymer degradation products was changed every other day.

2.7. Cellular uptake and fluorescence labeling of nanoparticles

Cellular uptake of the nanoparticles was also examined in vitro. hMSCs were seeded onto sterile cover slips at a density of 5000 cells/mL. Cells were allowed to attach and grow for 24 h before uptake studies were performed. The cover slips were washed with PBS and transferred into a Petri dish. After 4 h incubation with BPLP-co-PLGA50/50 nanoparticle solution (500 µg/mL), the medium was aspirated and the cells were washed three times with PBS to remove free nanoparticles. The cells were fixed with 4.0% paraformaldehyde solution for 2 h. After fixing, the cover slips were mounted on glass slides and imaged under a Leica DMLP fluorescence microscope (Leica Microsystems, Bannockburn, IL) equipped with a Nikon E500 Camera (8.4V, 0.9A, Nikon Corp., Japan).

2.8. In vivo foreign body response

To evaluate the in vivo host response, PLGA75/25 and BPLP-co-PLGA 75/25-100 disks (0.5–0.75 mm thickness and 8 mm diameter) were placed subcutaneously in 6-month-old female Sprague Dawley rats (Harlan Sprague Dawley, Inc., Indianapolis, IN) under deep isoflurane-O₂ general anesthesia. Animal experimentation was performed according to protocols approved by the Institutional Animal Care and Use Committee at the Pennsylvania State University. Rats were sacrificed with excess CO₂, and the copolymers with surrounding tissues were harvested and fixed by soaking in 10% formalin for 2 days. The samples were processed on an automated tissue processor, embedded in paraffin wax, and sectioned into 4 µm sections. Six slides from different areas of the explants were stained with hematoxylin and eosin staining (H & E staining) [34]. The cross-sections were examined using a Leica DMLP microscope (Leica Microsystems Inc., Bannockburn, IL) fitted with a Nikon E500 CCD camera (Nikon Corp., Japan). For quantitative analysis, all the cells in a 200 × 200 µm² region of the skin-side tissue near the implants from 400× images of H & E staining were counted. For one sample, at least 8 different square regions from different specimens were analyzed and the numbers were averaged.

2.9. Characterization of 5-fluorouracil (5-Fu) loaded nanoparticles

5-Fu calibration curve was established as follows: 10 mg of 5-Fu was dissolved in a 50 mL volumetric flask to obtain a final concentration of 0.2 mg/mL stock solution. The standard stock solution was diluted with water to obtain a series of standard solutions with various concentrations (0.1–100 µg/mL). The 5-Fu standard solutions were filtered through a 0.40 µm membrane before analysis. A Shimadzu high-performance liquid chromatography

(HPLC) system with UV detector was used for the analysis. A Phenomenex Kinex C18 column (4.6 × 150 mm, 5 µm) was used for separation. The column temperature was maintained at 25 °C. The standards and samples were determined using a mobile phase consisting of methanol and water (10:90, v/v) at a flow rate of 1.0 mL/min. The injection volume was 20 µL. The peak of 5-Fu was detected at the wavelength of 265 nm.

Measurement of 5-Fu encapsulation efficiency and loading content was conducted as follows: 5-Fu loaded nanoparticles solutions were ultra-speed centrifuged (25,000g for 30 min at 4 °C) twice, and each time the supernatant was collected. A Shimadzu UFLC system equipped with UV detector was used to test the 5-Fu absorbance in the supernatant as described above. The 5-Fu content in the supernatant was calculated based on the 5-Fu calibration curve. The encapsulation efficiency (EE%) and loading content (LC) of 5-Fu were calculated using Eqs. (2) and (3), respectively:

$$\text{EE}(\%) = (W_{\text{total}} - W_{\text{free}})/W_{\text{total}} \times 100 \quad (2)$$

$$\text{LC} = (W_{\text{total}} - W_{\text{free}})/W_{\text{NP}} \times 100 \quad (3)$$

where W_{total} and W_{free} are the total weight of initial 5-Fu and the weight of 5-Fu detected in supernatant after centrifugation, respectively. W_{NP} is the weight of copolymer in nanoparticle solutions.

In vitro drug release from 5-Fu loaded nanoparticles was studied in triplicate using a dialysis method with phosphate buffered saline (PBS, pH = 7.4) as the release medium. 5-Fu loaded PLGA 75/25 nanoparticles were chosen as control. Briefly, 50 mg of 5-Fu loaded nanoparticle powders was dispersed in 5.0 mL PBS (pH = 7.4) and placed into a dialysis membrane bag (with a molecular cut-off of 6.1 Kda, Spectra/Por® 6.1 kD dialysis membrane pre-wetted RC tubing; Spectrum, New Brunswick, NJ), tied and then incubated in a capped centrifuge tube containing 45 mL of PBS (pH = 7.4). The centrifuge tube was kept at 37 °C in a water bath on an orbital shaker that was under shaking at 120 rpm. At appropriate intervals, 2 mL release medium was extracted and 2 mL fresh PBS solution was replenished into the centrifuge tube right after sample withdrawal. The amount of 5-Fu in the release medium was analyzed by HPLC as described above. All measurements were performed in triplicate and the values were averaged.

3. Results and discussion

BPLP-co-PLGA copolymers were synthesized in two steps (Fig. 1a). First, a hydroxyl-terminated BPLP prepolymer was synthesized according to our previously published methods [19]. Then the hydroxyl-terminated BPLP (BPLP-Cys) prepolymers were used as macro-initiators to react with L-lactide and glycolide via a ring-opening polymerization catalyzed by stannous 2-ethylhexanoate in a flame sealed reactor under vacuum to give BPLP-co-PLGA. The obtained BPLP-co-PLGA copolymers exhibited inherent photoluminescence from BPLP [19], which enabled visualization by fluorescence imaging. Various BPLP-co-PLGA copolymers were synthesized with different molar feeding ratios of L-lactide to glycolide (LA/GA as 75:25 and 50:50) and different molar ratios of BPLP to total L-lactide and glycolide (BPLP/(LA + GA) of 1:50, 1:100, and 1:200). Pure PLGA copolymers with the same L-lactide to glycolide molar feeding ratios were also synthesized as controls. The resulting polymers with different feeding ratios, molecular weights (M_w), polydispersity indexes (M_w/M_n) and intrinsic viscosities ($[\eta]$) are summarized in Fig. 1b. The average molecular weight (M_w) was 8650, 19,730, 26,090 and 30,090 g/mol for BPLP-co-PLGA 75/25-50 (LA/GA = 72/25, BPLP/(LA + GA) = 50), BPLP-co-PLGA 75/25-100, BPLP-co-PLGA 75/25-200 and PLGA 75/25, respectively. The average molecular weight (M_w) was 8240, 18,270, 23,690 and 25,460 g/mol for

BPLP-co-PLGA 50/50-50, BPLP-co-PLGA 50/50-100, BPLP-co-PLGA 50/50-200 and PLGA 50/50, respectively. The molecular weights of the copolymers correlated well with BPLP/(LA + GA) ratios: the molecular weight decreased with the increase of the ratio of BPLP/(LA + GA). BPLP also acted as a molecular weight controller in the synthesis of BPLP-co-PLGA copolymers. It was found that the LA/GA molar ratio also impacted the molecular weight of the synthesized copolymers. With the introduction of the same molar ratio of BPLP, molecular weight decreased with the increase of the molar percentage of glycolide in (LA + GA) (Fig. S1). The relationship between the intrinsic viscosity of the synthesized copolymers and the molar ratio of BPLP/(LA + GA) is illustrated in Fig. S2. The impact of the molar ratio of BPLP/(LA + GA) on the intrinsic viscosity was similar to that on the molecular weight, which verified that control of molecular weight could be achieved by adjusting the amount of BPLP in the synthesis of BPLP-co-PLGA copolymers.

¹H NMR spectra of PLGA and BPLP-co-PLGA verified the successful incorporation of BPLP into the PLGA copolymer matrix (Fig. 2a), as indicated by the appearance of signals located between 4.0 and 4.30 ppm (a), which were assigned to the protons in –CH₂O– from 1, 8-octanediol in BPLP. The signals at ~5.2 ppm (b and d) and ~4.6–4.9 ppm (c and e) were attributed to the protons from lactic acid –CH– and the glycolic acid –CH₂– respectively, randomly distributed in the copolymer backbone. The ratios of the signal intensity of the characteristic proton peaks from related chemical compositions of PLGA 75/25 and various BPLP-co-PLGA copolymers were calculated (Fig. S3a–e, Supporting information). The resulting compositions of the synthesized copolymers were well correlated to the feeding ratios between BPLP, LA and GA (Fig. S3f, Supporting information). The actual composition of BPLP-co-PLGA copolymers could be well controlled by varying the feeding ratios of raw materials, including BPLP (as an initiator) and monomers. It could be deduced that when the number of protons from –CH₂O– in 1,8-octanediol of BPLP (α in Fig. S3f) was around 20 (meaning that the polymerization degree of BPLP was around 5, which is in accordance with our previous molecular weight characterization [19]), the determined compositions of BPLP/(LA + GA) were 1/199.52, 1/100.5, 1/49.0 and 1/104.98 for BPLP-co-PLGA 75/25-200, BPLP-co-PLGA 75/25-100, BPLP-co-PLGA 75/25-50 and BPLP-co-PLGA 50/50-100, respectively, which matched the designed compositions of 1/200, 1/100, 1/50, and 1/100 very well. Similar ATR-FTIR spectrums of BPLP-co-PLGA and PLGA (with characteristic absorption of ester groups at 1745 cm⁻¹) further confirmed their similar chemical structure, given the fact that BPLP only took up a small portion in BPLP-co-PLGA copolymer (Fig. 2b).

The thermal properties of representative PLGA and BPLP-co-PLGA copolymers were determined by differential scanning calorimetry (DSC) and thermal gravimetric analysis (TGA). The glass transition temperatures (T_g s) of copolymers were indicated by the DSC curves (Fig. 2e). The T_g values of PLGA 75/25, BPLP-co-PLGA 75/25-200, BPLP-co-PLGA 75/25-100 and BPLP-co-PLGA 75/25-50 were 39.5, 35.6, 32.5 and 30.2 °C, respectively. Clearly, the T_g value decreased with an increase of the incorporation ratio of the sticky and soft BPLP chain (Fig. S4, Supporting information). The T_g s of PLGA 50/50 and BPLP-co-PLGA 50/50-100 were 19.3 and 17.9 °C, respectively, also displaying a similar T_g decreasing tendency. It was also found that T_g values of PLGA and BPLP-co-PLGA increased with increasing ratios of LA/GA in the copolymers. Higher LA percentage brought more rigid L-methyl side groups, which would produce a stronger steric hindrance effect, reducing the flexibility of the copolymer chain, thus increasing the T_g s of the copolymers. Moreover, the T_g s of BPLP-co-PLGA 75/25-200 and BPLP-co-PLGA 75/25-100 copolymers were 35.6 and 32.5 °C, respectively, just below body temperature (37 °C). Thus, these copolymers would stay in a viscoelastic state when applied

in vivo. A viscoelastic copolymer matrix can have a higher permeability to water compared with rigid polymers, which may lead to improved hydration, degradation and drug release rate. TGA curves of BPLP-co-PLGA 75/25-50, BPLP-co-PLGA 75/25-100, BPLP-co-PLGA 75/25-200 and PLGA75/25 copolymers are presented (Fig. 2f) and the related analysis results are also summarized (Table S2, Supporting information). The onset mass loss temperatures for BPLP-co-PLGA 75/25-50, BPLP-co-PLGA 75/25-100 and BPLP-co-PLGA 75/25-200 copolymers were all about 100 °C, while the start of thermal decomposition for PLGA 75/25 copolymers occurred at around 140 °C, which demonstrates that the incorporation of BPLP lowered the thermal stability of the copolymers. The temperatures at 5%, 10% and 100% mass loss further confirmed that increased BPLP incorporation lowers the thermal stability of the copolymers.

The mechanical properties of PLGA and BPLP-co-PLGA copolymer films were investigated through tensile testing. The results are shown in Fig. 2c (tensile strength and Young's modulus values) and Fig. 2d (stress-strain curves). The detailed mechanical properties of PLGA and BPLP-co-PLGA copolymer films are also summarized and listed in Table S1 (Supporting information). The tensile strength and the Young's modulus of BPLP-co-PLGA 75/25 series copolymer films were 14.955 ± 2.992 MPa and 72.083 ± 3.859 MPa, 13.185 ± 0.894 MPa and 66.643 ± 3.359 MPa, and 5.078 ± 0.112 MPa and 22.663 ± 1.282 MPa for 1/200, 1/100 and 1/50 feeding ratios of BPLP/(LA + GA), respectively. The tensile strength and the Young's modulus greatly decreased when BPLP/(LA + GA) increased from 1/100 to 1/50. PLGA films exhibited a slightly higher but comparable tensile strength and Young's Modulus (15.347 ± 1.403 MPa and 74.949 ± 5.429 MPa) compared to their BPLP-co-PLGA counterparts. Similar phenomena could be seen in the BPLP-co-PLGA 50/50 series copolymer films. However, the tensile strength and Young's modulus of BPLP-co-PLGA 75/25 series were much higher than those of corresponding BPLP-co-PLGA 50/50 series due to the higher content of LA as hard segments. All BPLP-co-PLGA copolymers exhibited the characteristics of plastic polymers similar to PLGA copolymers, although there are no obvious yield points in their stress-strain curves (in contrast to PLGA). A decrease of the BPLP/(LA + GA) ratio resulted in a decrease of elongation at break. When the ratio of BPLP/(LA + GA) decreased from 1/100 to 1/200, the elongation at break of BPLP-co-PLGA 75/25 series and BPLP-co-PLGA 50/50 series dramatically decreased from 219.37 ± 24.45% to 85.80 ± 8.98% and 260.43 ± 29.78% to 156.74 ± 23.93%, respectively. BPLP-co-PLGA films with BPLP/(LA + GA) of 1/100 and their PLGA counterparts showed comparable elongations at break and similar stress-strain curves.

The equilibrium water-in-air contact angles vs. time curves of PLGA 75/25 and BPLP-co-PLGA 75/25-100 copolymer films were plotted to analyze the surface properties (Fig. 2g). It was shown that water droplets had slightly lower contact angles on BPLP-co-PLGA 75/25-100 film than on PLGA75/25 film. The initial water contact angle of BPLP-co-PLGA 75/25-100 film was about 71.5° followed by a quick decrease through the first 30 min and then an almost equilibrium contact angle of about 60° was observed, a trend which was comparable with the water contact angle of PLGA75/25 film. A decrease of water droplet volumes occurred during the 75 min test, which is attributed to water adsorption in polymer films and also some water evaporation. The contact angle results confirm that BPLP-co-PLGA 75/25-100 exhibits better wettability than PLGA 75/25, which may be favorable for cell adhesion, drug encapsulation and release properties [32].

The photoluminescence of the obtained PLGA and BPLP-co-PLGA copolymers was evaluated and the excitation and emission spectra are depicted (Fig. 3a). Obviously, PLGA itself has no photoluminescence, while all BPLP-co-PLGA copolymers showed significant photoluminescence and possess the same maximum

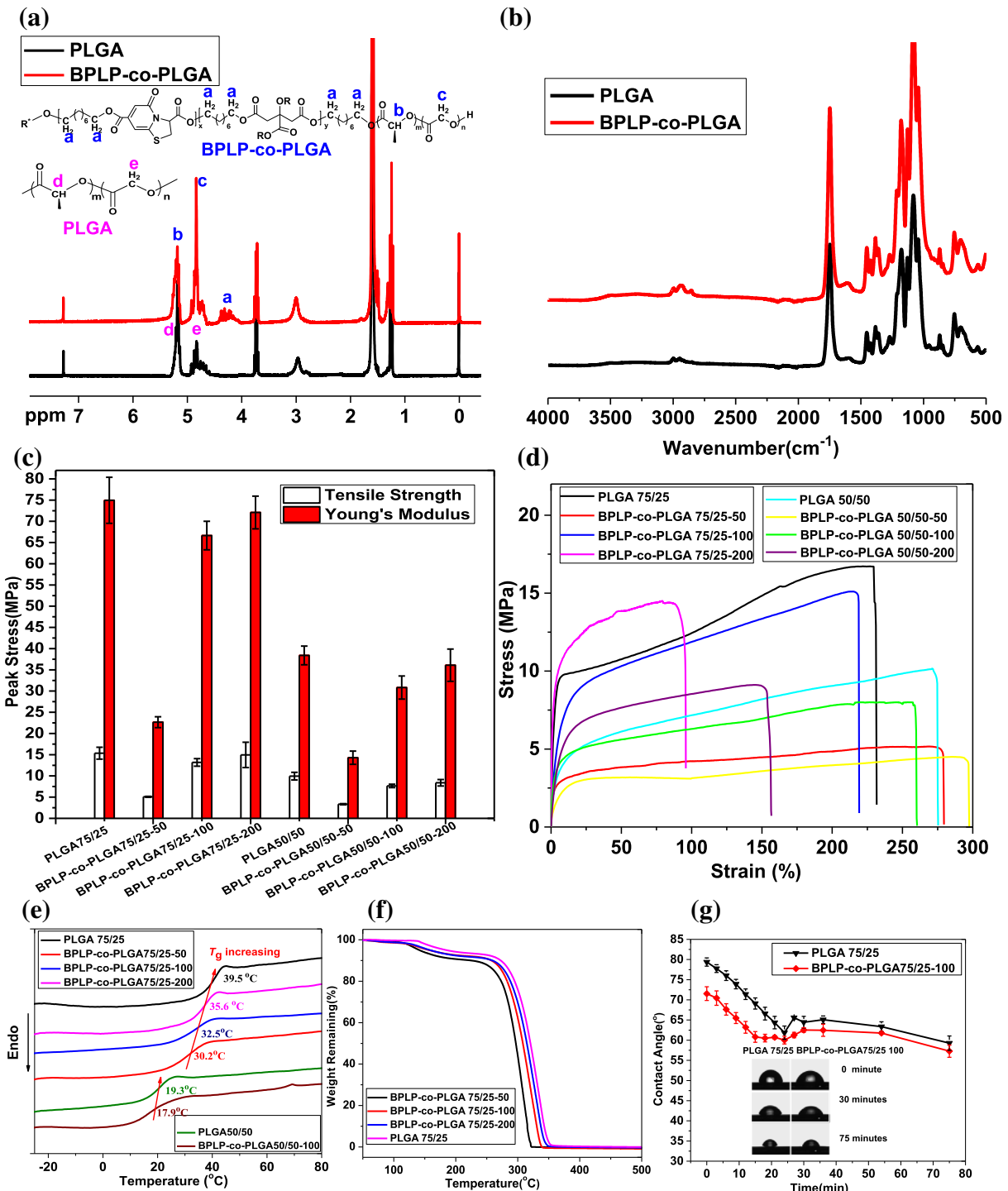


Fig. 2. Chemical, mechanical and thermodynamic properties and wettability of BPLP-co-PLGA. ^1H NMR (a) and ATR-FTIR (b) spectra, tensile strength and Young's modulus (c), strain-stress curves (d), differential scanning calorimetry (DSC, e) and thermal gravity analysis (TGA, f) curves of representative PLGA and BPLP-co-PLGA. Water-in-air contact angle vs. time curves (g) of representative PLGA and BPLP-co-PLGA copolymers films.

excitation (368 nm) and emission (434 nm) wavelengths as BPLP. Since BPLP is the fluorophore, emission intensity of BPLP-co-PLGA copolymers increased with the increase of the molar ratio of BPLP to (LA + GA) in BPLP-co-PLGA copolymers (Fig. S5, Supporting information). Moreover, BPLP-co-PLGA copolymers possessed much better photostability than commercial organic dyes such as rhodamine B (Fig. 3b) under continuous ultraviolet (UV) light illumination. BPLP-co-PLGA copolymers also displayed

high quantum yields and extinction coefficients, comparable to other polymeric photoluminescent materials, such as poly(amido amine)s [35,36], which further demonstrated the strong photoluminescence of BPLP-co-PLGA copolymers (Fig. 3c and d). BPLP-co-PLGA 75/25-100 films showed strong fluorescence emission under UV light and fluorescence microscope with GFP, Cy3 and DAPI filters (Fig. 3e). BPLP-PLGA copolymers have brightness intensities in the range of 6550–19,230, which are comparable to

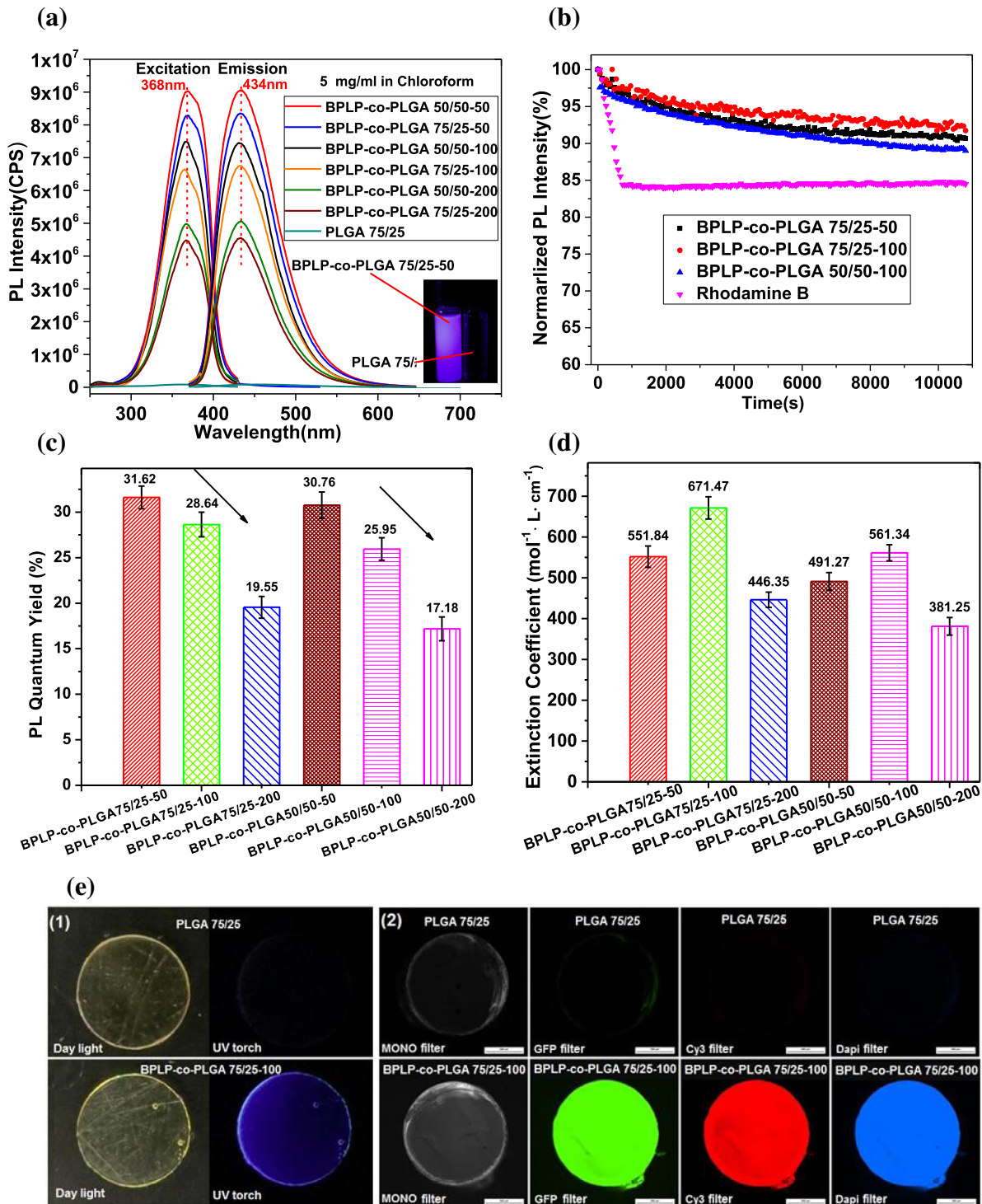


Fig. 3. Photoluminescent (PL) properties of BPLP-co-PLGA solutions, films. (a) Photoluminescent excitation and emission spectra of BPLP-co-PLGA copolymers solutions (5 mg/mL in chloroform) (insert, optical imaging of BPLP-co-PLGA 75/25-100 solution under UV light), PLGA 75/25 was used as control. (b) Photoluminescence stability evaluation of representative BPLP-co-PLGA copolymers and rhodamine B. (c) and (d) Quantum yields and extinction coefficients of BPLP-co-PLGA copolymers. (e) Imaging effect of PLGA 75/25 and BPLP-co-PLGA 75/25-100 films (1) under white or UV light, (2) under fluorescent microscope with mono filter, GFP filter, Cy3 filter and DAPI filter.

that of some frequently used small molecular organic dyes including Alexa Fluor 430 (8800) and even DAPI (15,660) [37]. These photoluminescent properties make BPLP-co-PLGA copolymers promising biomaterials for applications such as tissue engineering and drug delivery where fluorescent properties are desired.

Degradation study in PBS for representative PLGA and BPLP-co-PLGA copolymers was conducted and the corresponding degra-

tion profiles are shown in Fig. 4a. It was observed that BPLP-co-PLGA 75/25-100, BPLP-co-PLGA 75/25-200 and PLGA 75/25 underwent a very similar degradation process and the increased incorporation of BPLP slightly accelerated the degradation rate of BPLP-co-PLGA copolymers due to the slight increase in hydrophilicity. The fact that BPLP-co-PLGA 50/50-100 degraded much faster than BPLP-co-PLGA 75/25-100 showed that the

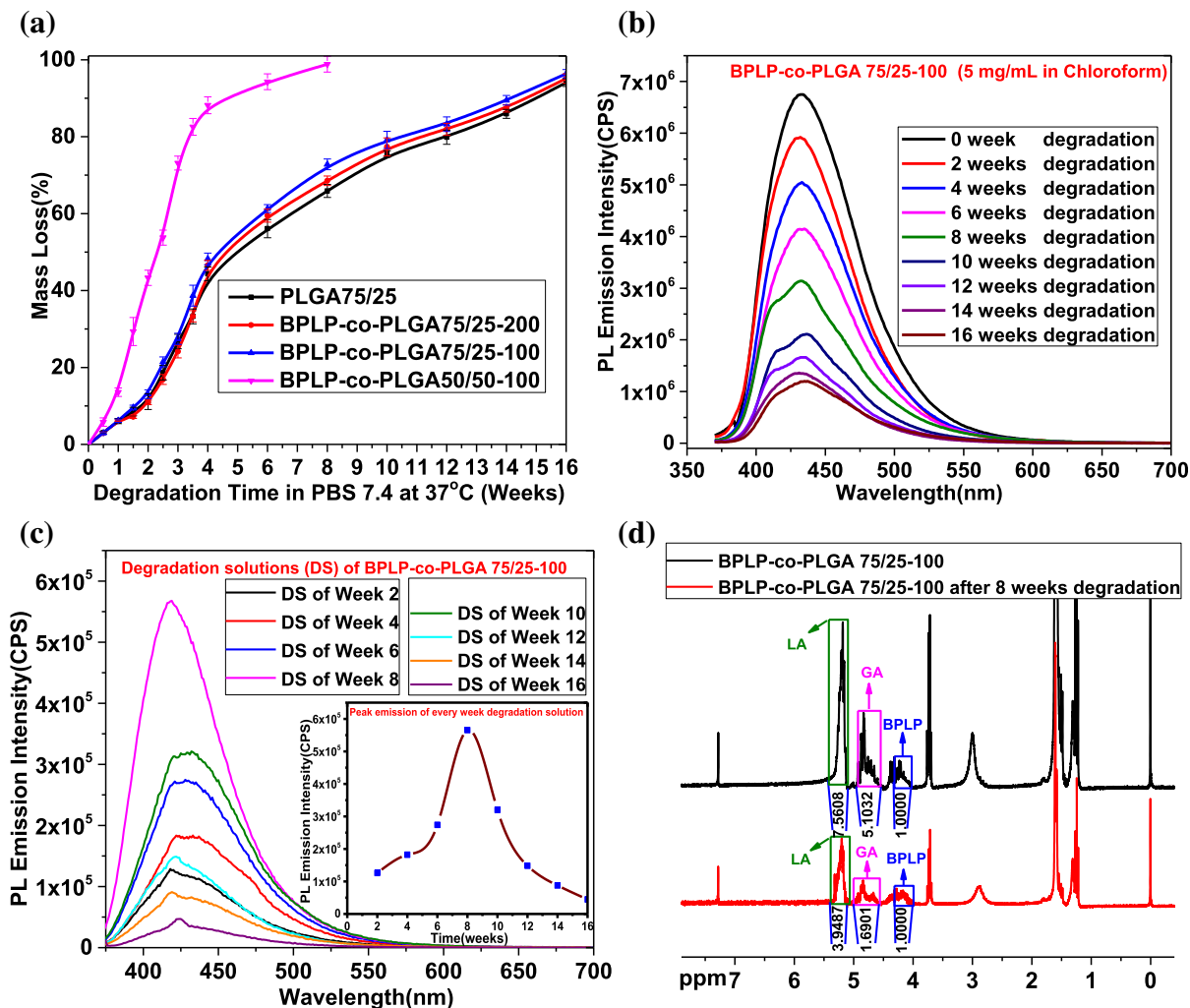


Fig. 4. In vitro degradation of BPLP-co-PLGA. (a) Weight loss in PBS (pH 7.4) of BPLP-co-PLGA and PLGA 75/25 copolymers at 37 °C. (b) Photoluminescent emission spectra of BPLP-co-PLGA 75/25-100 copolymers (5 mg/mL in chloroform) at various times degradation in PBS. (c) Photoluminescence emission spectra of degradation solutions (DS) of BPLP-co-PLGA 75/25-100 (insert: emission intensity vs. degradation time). (d) ¹H NMR spectra of original and degrading (6 weeks in PBS) BPLP-co-PLGA 75/25-100.

increase of hydrophilic GA content greatly increased the degradation rate of BPLP-co-PLGA copolymers. The degradation rate could be easily adjusted by varying the feeding composition ratio to meet the application requirements. The photoluminescence emission intensity of BPLP-co-PLGA 75/25-100 copolymer decreased with increasing degradation time and the emission peaks always showed up at the same wavelength of 434 nm during degradation (Fig. 4b). Noteworthy, it was also found that the photoluminescence emission peak intensity retaining percentage remained higher than the mass remaining percentage of BPLP-co-PLGA 75/25-100 copolymer in the process of degradation. The photoluminescence intensity retained was about 17.63% even when the mass remaining was about 3.62% at the degradation time of 16 weeks (Fig. S6, Supporting information). The photoluminescence emission intensity of PBS solutions in the process of BPLP-co-PLGA 75/25-100 degradation was tracked weekly to investigate the degradation rate as a function of time of BPLP in BPLP-co-PLGA 75/25-100 (Fig. 4c). It could be seen that the fastest degradation rate for BPLP in BPLP-co-PLGA 75/25-100 should occur around the time of the 8th week. The comparison between the ¹H NMR spectra of original BPLP-co-PLGA 75/25-100 copolymer and BPLP-co-PLGA 75/25-100 after 6 weeks degradation showed significant changes in the molar ratios of LA to GA and BPLP to (LA + GA) (Fig. 4d). After 6 weeks degradation of BPLP-co-PLGA 75/25-100,

the ratio of signal intensity for BPLP/LA/GA changed from the original 1/7.5608/5.1032 to 1/3.9487/1.6901. The actual molar ratios of LA to GA and BPLP to (LA + GA) increased from 74.76/25.23 to 82.37/17.63 and from (1/α)/5.056 to (1/α)/2.397, respectively (Table S3, Supporting information, α means number of protons from -CH₂O- in 1,8-octanediol of BPLP). The results demonstrated that in the copolymer chain of BPLP-co-PLGA 75/25-100, the GA segment degraded fastest and the BPLP segment degraded slowest. The degradation behavior of BPLP-co-PLGA indicates that strong and stable photoluminescence as an inherent characteristic will be preserved in almost the entire lifetime of BPLP-co-PLGA till complete degradation, which is different from our previous studies on BPLP-co-PLLA from which the percentage of fluorescence signal loss of BPLP-co-PLLA20 closely matches the percentage of in vitro weight loss of polymer due to the relatively similar degradation rate of BPLP and PLLA [21]. The above results suggest that the correlation between fluorescence signal loss and material's degradation can be controlled by selecting the degradation rates of non-fluorescent sections of the co-polymers. Anyhow, understanding the relationships of fluorescence signal decay and material degradation is a key to enabling non-invasive material visualization and degradation tracking through fluorescence imaging.

In vitro cell cytotoxicity of BPLP-co-PLGA films and degradation products, bio-imaging effect by cellular uptake of BPLP-co-PLGA

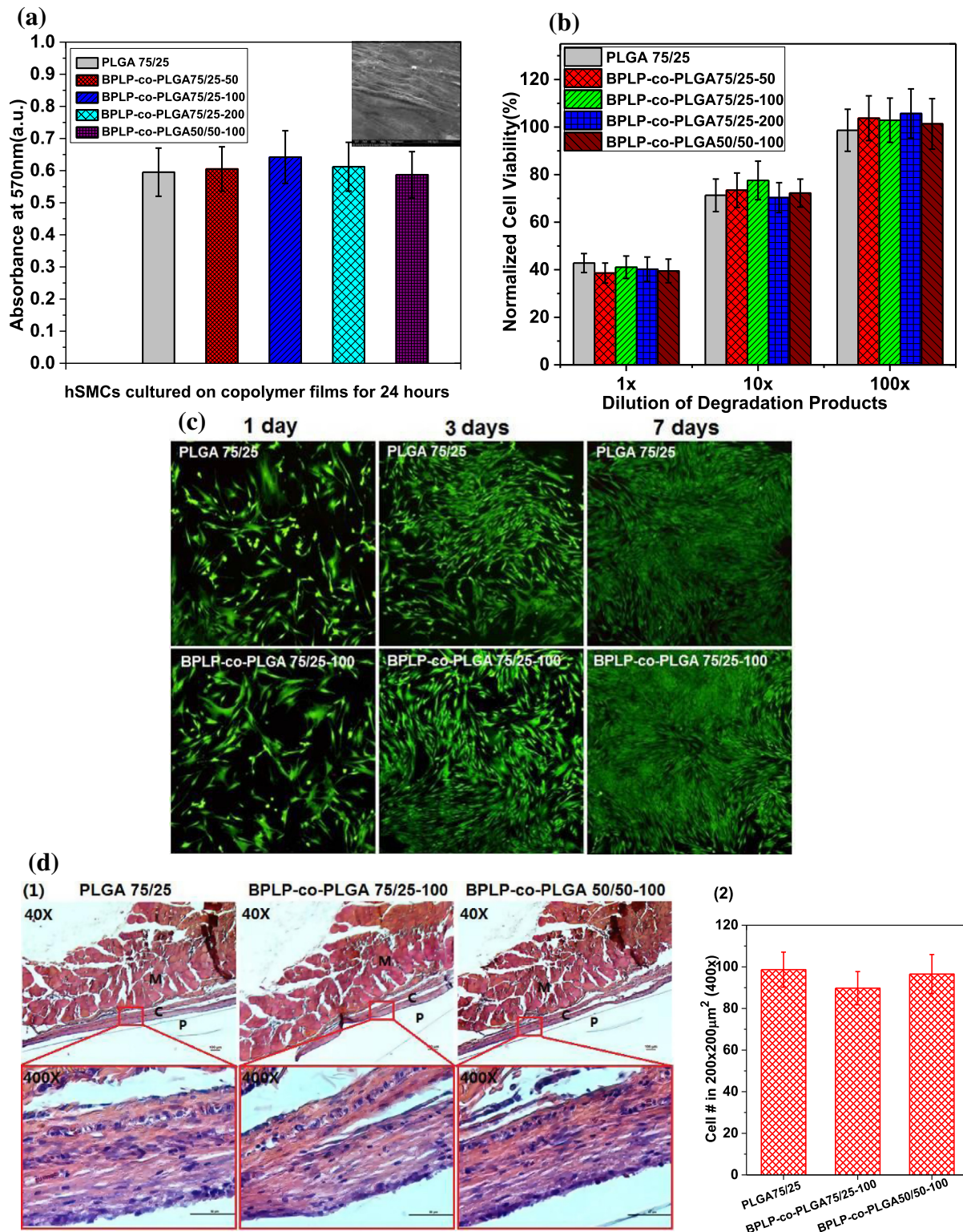


Fig. 5. In vitro cytotoxicity and in vivo foreign body responses of BPLP-co-PLGA. (a) MTT assay (570 nm) against human mesenchymal stem cells (hMSCs) cultured on copolymer films for 24 h (insert, SEM image of hMSCs cultured for 24 h on BPLP-co-PLGA 75/25-100 film). (b) Normalized cell viability of hMSCs cultured with the presence of different dilutions of BPLP-co-PLGA degradation products, PLGA 75/25 was used as control. (c) Live/dead assay images of hMSCs cultured with 10 \times diluted degradation products of PLGA 75/25 and BPLP-co-PLGA 75/25-100 for 1, 3 and 7 days. (d) Foreign body response evaluations: (1) Representative H & E staining images of surrounding tissues of BPLP-co-PLGA and PLGA copolymer films after 1 month of implantation (P: polymer, C: fibrous capsule, M: muscle); (2) cell numbers in a 200 \times 200 μm^2 square region (from 400 \times images of H & E staining) of the skin-side tissue near the implants.

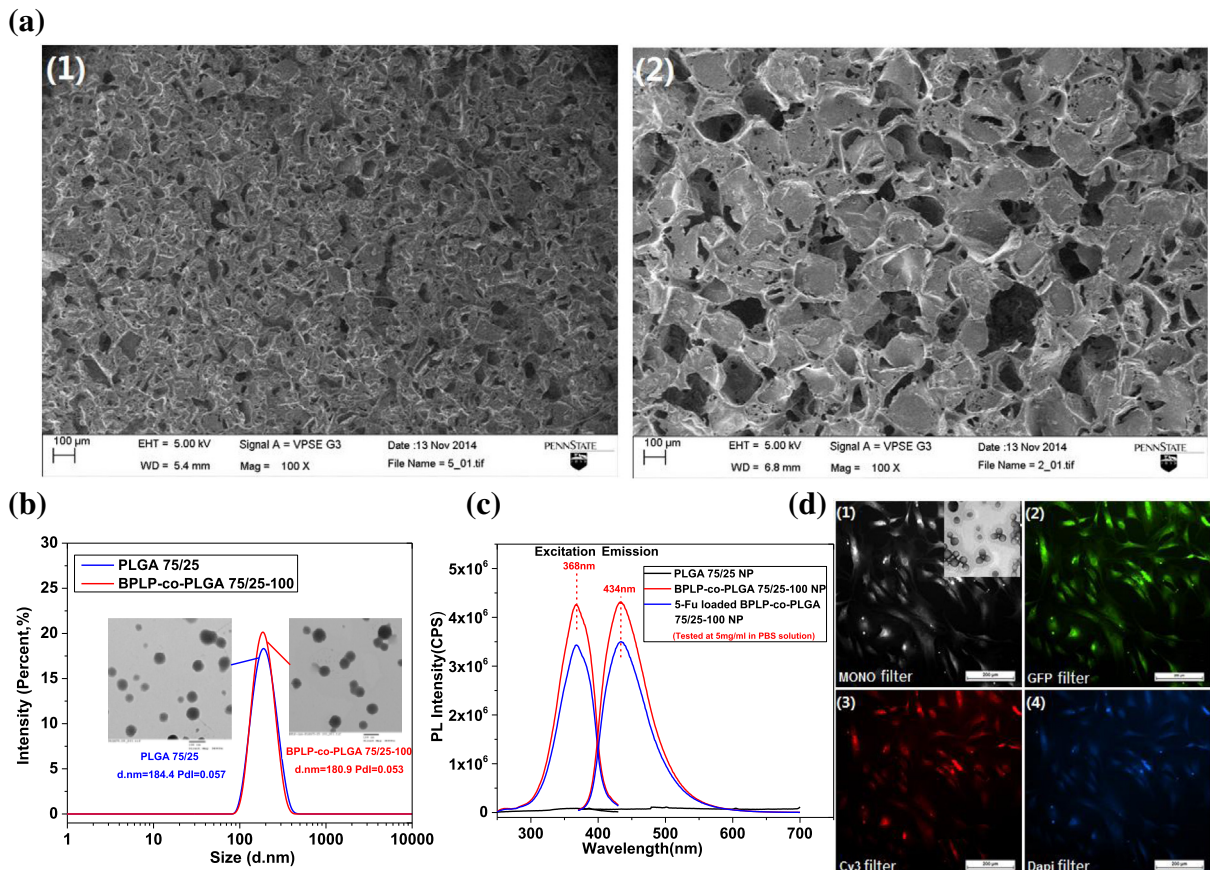


Fig. 6. Scaffold and nanoparticle fabrication of BPLP-co-PLGA. (a) SEM images of BPLP-co-PLGA 75/25-100 scaffolds with pore sizes of 50–100 μm (1), and 200–250 μm (2). (b) The particle sizes and distributions of representative PLGA and BPLP-co-PLGA nanoparticle dispersions (insert: TEM images of corresponding nanoparticles). (c) Excitation and emission spectra of BPLP-co-PLGA 75/25-100 nanoparticles, 5-Fu loaded BPLP-co-PLGA 75/25-100 nanoparticles and control PLGA 75/25 nanoparticles with a concentration of 5 mg/mL in PBS solution. (d) BPLP-co-PLGA 75/25-50 nanoparticle (500 μg/mL)-uptaken hMSCs observed under fluorescence microscope with (1) Monochrome filter (insert, TEM image of BPLP-co-PLGA 75/25-50 nanoparticles, particle size: 110 nm), (2) GFP filter, (3) Cy3 filter, and (4) DAPI filter.

nano-particles and the in vivo foreign body response to BPLP-co-PLGA implants were evaluated (Fig. 5). The comparable cell viability on all films by MTT assay and the stretched morphology of cells on BPLP-co-PLGA75/25-100 film by SEM indicate that BPLP-co-PLGA supported human mesenchymal stem cells (hMSCs) adhesion and proliferation and exhibited a cytotoxicity in vitro similar to that of PLGA (Fig. 5a). The normalized cell viabilities of hMSCs cultured in the presence of PLGA or BPLP-co-PLGA degradation products were all around 40%, 75% and 100% for 1×, 10× and 100× dilutions, respectively (Fig. 5b). The results illustrate that both PLGA and BPLP-co-PLGA degradation products had a dose-dependent cytotoxicity comparable to one another. The Live/Dead assay images of hSMCs cultured with 10× dilutions of PLGA and BPLP-co-PLGA degradation products both display a robust growth trend from day 1 to day 7, which further confirmed the biocompatibility of BPLP-co-PLGA (Fig. 5c). In order to study the in vivo foreign body response, representative BPLP-co-PLGA copolymer films and PLGA films (as controls) were implanted in vivo to assess the cell behavior of tissue surrounding the implants using H & E staining. All samples implanted for 1 month produced a thin fibrous capsule between the copolymer film and muscle indicating minimal inflammatory reactions. The cell density around all implants was also similar and BPLP-co-PLGA implant samples did not elicit more severe foreign body reactions than the PLGA implant sample (Fig. 5d). The results of cytotoxicity and in vivo biocompatibility studies strongly demonstrated that incorporating BPLPs into PLGAs does not compromise the cyto/tissue-compatibility

of the materials, thus meriting BPLP-PLGAs for future biomedical applications.

To verify the application potential of our BPLP-PLGA copolymers in tissue engineering and drug delivery, BPLP-co-PLGA porous scaffolds and nanoparticles were fabricated. BPLP-co-PLGA porous scaffolds with controlled pore sizes (here, 50–125 μm or 250–425 μm) and porosity and high interconnectivity were fabricated via a conventional salt-leaching method. The SEM images of the obtained scaffolds are shown in Fig. 6a. BPLP-co-PLGA nanoparticles were fabricated using a convenient oil in water (O/W) emulsion evaporation method, and the size, size distribution, and morphology of so-obtained nanoparticles were investigated (Fig. 6b). The average size of PLGA 75/25 and BPLP-co-PLGA 75/25-100 nanoparticles measured by dynamic light scattering (DLS) were 184.4 and 180.9 nm, respectively, and both of them were dispersed very evenly with polydispersity index (PDIs) of 0.057 and 0.053 respectively. The above results were also confirmed by TEM observation (insert images in Fig. 6b). BPLP-co-PLGA 75/25-100 nanoparticles in phosphate buffered saline (PBS, pH = 7.4) solution still exhibited strong and stable photoluminescent performance (Fig. 6c). Cellular uptake of the BPLP-co-PLGA nanoparticles was conducted. The fluorescent images of BPLP-co-PLGA 75/25-50 nanoparticles (average size about 110 nm) taken up by hMSCs were also recorded, confirming the cell labeling ability of the nanoparticles (Fig. 6d).

To validate the theranostic potential of BPLP-co-PLGA, 5-fluorouracil (5-Fu), an anti-tumor agent, was selected as a model

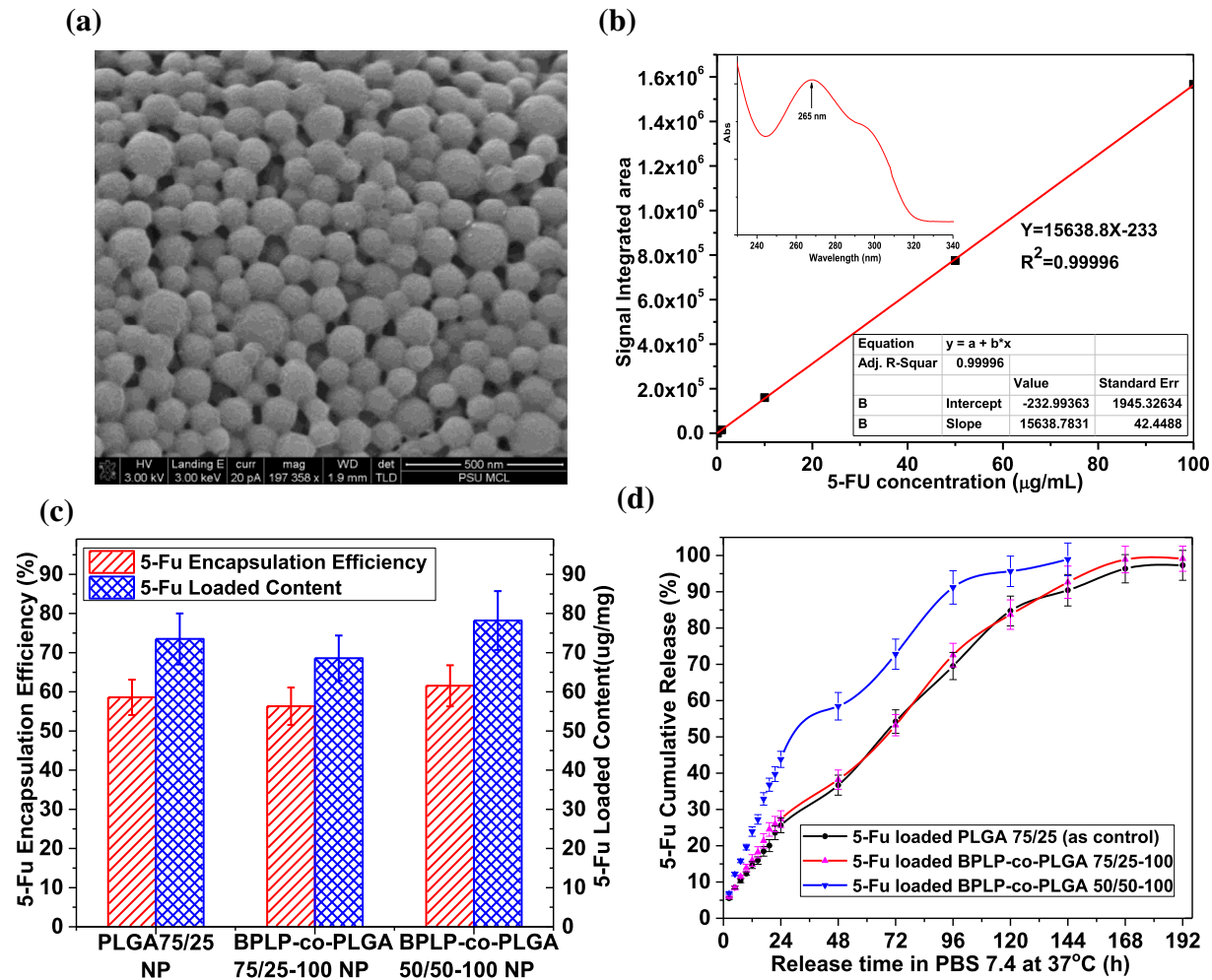


Fig. 7. Drug loading and release study of BPLP-co-PLGA nanoparticles. (a) SEM image of 5-fluorouracil (5-Fu) loaded BPLP-co-PLGA 75/25-100 nanoparticles. (b) Standard curve of 5-Fu obtained by high-performance liquid chromatography (HPLC) (insert, UV-vis curve of 5-Fu). (c) 5-Fu encapsulation efficiency and loaded contents in PLGA and BPLP-co-PLGA nanoparticles. (d) Complete release profiles of 5-Fu from 5-Fu loaded PLGA nanoparticles (as control) and 5-Fu loaded BPLP-co-PLGA nanoparticles in PBS (pH 7.4) at 37 °C.

drug to evaluate the drug encapsulation and release capability of BPLP-co-PLGA nanoparticles. 5-Fu loaded BPLP-co-PLGA 75/25-100 nanoparticles still exhibited strong photoluminescence when dispersed in PBS as shown in Fig. 6c. The SEM images of 5-Fu loaded BPLP-co-PLGA 75/25-100 nanoparticles confirmed that these particles displayed relatively regular spherical morphology with a consistent surface and an even size distribution of 100–150 nm which avoided a burst release after encapsulation (Fig. 7a). The encapsulation efficiency and load content of representative PLGA and BPLP-co-PLGA nanoparticles against 5-Fu (Fig. 7c) were determined using a 5-Fu standard curve obtained by HPLC (Fig. 7b). The results revealed that higher molar content of GA in BPLP-co-PLGA resulted in higher encapsulation efficiency and load content due to an improvement in hydrophilicity, which led to more encapsulation of water soluble 5-Fu (Fig. 7c). The release profiles of 5-Fu from 5-Fu loaded PLGA as control and 5-Fu loaded BPLP-co-PLGA nanoparticles in PBS at 37 °C were studied (Fig. 7d). 5-Fu encapsulated within PLGA and BPLP-co-PLGA nanoparticles experienced a relatively sustained release during the following 6–8 days. The release profiles illustrate that although all 5-Fu loaded PLGA and BPLP-co-PLGA nanoparticles exhibited a burst release in the first 24 h, they then underwent a slow continuous release in the following days. 5-Fu loaded PLGA 75/25 nanoparticles and 5-Fu loaded BPLP-co-PLGA 75/25-100 nanopar-

ticles exhibited very similar release profiles. While the released amount and rate of 5-Fu from BPLP-co-PLGA 50/50-100 nanoparticles was much faster than that from BPLP-co-PLGA 75/25-100 nanoparticles, which could be explained by the higher percentage of hydrophilic GA in BPLP-co-PLGA 50/50-100 than in BPLP-co-PLGA 75/25-100 leading to faster hydration, faster biodegradation and lower glass transition temperature. The in vitro drug loading and release studies demonstrated that BPLP-co-PLGA could be used as multifunctional nano-reservoir systems to control on-demand drug release.

4. Conclusion

We have synthesized and characterized a novel series of biodegradable photoluminescent polymer-poly(lactide-co-glycolide) (BPLP-co-PLGA) copolymers. BPLP-co-PLGAs possess inherent photoluminescence from BPLP and favorable mechanical properties, cyto-/tissue-compatibility and tailored biodegradability from PLGA. These copolymers can be easily fabricated into various morphologies such as films, nanoparticles and porous scaffolds while enabling fluorescence imaging capability. BPLP-co-PLGA is a new class of biodegradable photoluminescent polymers with potential in a wide range of biomedical applications where fluorescence

labeling and imaging are becoming enabling tools such as tissue engineering and cancer drug delivery and imaging.

Acknowledgements

This work was supported in part by National Institutes of Health Awards of the United States (to J.Y., NIBIB EB012575, NCI CA182670, NHLBI HL118498), the International Science & Technology Cooperation Program of Guangzhou, China (to J.H., 2012J5100043) and a project supported by Key Laboratory of New Lithium-ion Battery and Mesoporous Materials of Shenzhen, China (to J.H., 20120213).

Appendix A. Supplementary data

Supplementary data associated with this article can be found, in the online version, at <http://dx.doi.org/10.1016/j.actbio.2015.10.010>.

References

- [1] F.R. Maia, S.J. Bidarra, P.L. Granja, C.C. Barrias, Functionalization of biomaterials with small osteoinductive moieties, *Acta Biomater.* 9 (2013) 8773–8789.
- [2] N. Huebsch, D.J. Mooney, Inspiration and application in the evolution of biomaterials, *Nature* 462 (2009) 426–432.
- [3] L.S. Nair, C.T. Laurencin, Biodegradable polymers as biomaterials, *Prog. Polym. Sci.* 32 (2007) 762–798.
- [4] J. Guo, Z. Xie, R.T. Tran, D. Xie, D. Jin, X. Bai, et al., Click chemistry plays a dual role in biodegradable polymer design, *Adv. Mater.* 26 (2014) 1906–1911.
- [5] Q. Liu, L. Jiang, R. Shi, L. Zhang, Synthesis, preparation, in vitro degradation, and application of novel degradable bioelastomers—A review, *Prog. Polym. Sci.* 37 (2012) 715–765.
- [6] D. Xie, J. Guo, M.R. Mehdizadeh, R.T. Tran, R. Chen, D. Sun, et al., Development of injectable citrate-based bioadhesive bone implants, *J. Mater. Chem. B* 3 (2015) 387–398.
- [7] K. Ren, C. He, C. Xiao, G. Li, X. Chen, Injectable glycopolyptide hydrogels as biomimetic scaffolds for cartilage tissue engineering, *Biomaterials* 51 (2015) 238–249.
- [8] S.M. Giannitelli, P. Mozetic, M. Trombetta, A. Rainer, Combined additive manufacturing approaches in tissue engineering, *Acta Biomater.* 24 (2015) 1–11.
- [9] X. Michalet, F.F. Pinaud, L.A. Bentolila, J.M. Tsay, S. Doose, J.J. Li, et al., Quantum dots for live cells, *in vivo* imaging, and diagnostics, *Science* 307 (2005) 538–544.
- [10] J.O. Escobedo, O. Rusin, S. Lim, R.M. Strongin, NIR dyes for bioimaging applications, *Curr. Opin. Chem. Biol.* 14 (2010) 64–70.
- [11] R.A. Petros, J.M. DeSimone, Strategies in the design of nanoparticles for therapeutic applications, *Nat. Rev. Drug Discov.* 9 (2010) 615–627.
- [12] S.M. Maria, C. Prukner, Z. Sheikh, F.A. Müller, S.V. Komarova, J.E. Barralet, Characterization of biomimetic calcium phosphate labeled with fluorescent dextran for quantification of osteoclastic activity, *Acta Biomater.* 20 (2015) 140–146.
- [13] W. Wang, J. Liu, C. Li, J. Zhang, J. Liu, A. Dong, et al., Real-time and non-invasive fluorescence tracking of *in vivo* degradation of the thermosensitive PEGylated polyester hydrogel, *J. Mater. Chem. B* 2 (2014) 4185.
- [14] N. Artzi, N. Oliva, C. Puron, S. Shitreet, S. Artzi, A. bon Ramos, et al., In vivo and *in vitro* tracking of erosion in biodegradable materials using non-invasive fluorescence imaging, *Nat. Mater.* 10 (2011) 704–709.
- [15] J.K. Jaiswal, H. Mattossi, J.M. Mauro, S.M. Simon, Long-term multiple color imaging of live cells using quantum dot bioconjugates, *Nat. Biotechnol.* 21 (2003) 47–51.
- [16] T. Jamieson, R. Bakhshi, D. Petrova, R. Pocock, M. Imani, A.M. Seifalian, Biological applications of quantum dots, *Biomaterials* 28 (2007) 4717–4732.
- [17] Y.G. Yanushevich, D.B. Staroverov, A.P. Savitsky, A.F. Fradkov, N.G. Gurskaya, M.E. Bulina, et al., A strategy for the generation of non-aggregating mutants of anthozoa fluorescent proteins, *FEBS Lett.* 511 (2002) 11–14.
- [18] Y. Zhang, J. Yang, Design strategies for fluorescent biodegradable polymeric biomaterials, *J. Mater. Chem. B* 1 (2013) 132–148.
- [19] J. Yang, Y. Zhang, S. Gautam, L. Liu, J. Dey, W. Chen, et al., Development of aliphatic biodegradable photoluminescent polymers, *Proc. Natl. Acad. Sci. U.S.A.* 106 (2009) 10086–10091.
- [20] Y. Zhang, R.T. Tran, I.S. Qattan, Y.T. Tsai, L. Tang, C. Liu, et al., Fluorescence imaging enabled urethane-doped citrate-based biodegradable elastomers, *Biomaterials* 34 (2013) 4048–4056.
- [21] Z. Xie, Y. Zhang, L. Liu, H. Weng, R.P. Mason, L. Tang, et al., Development of intrinsically photoluminescent and photostable polylactones, *Adv. Mater.* 26 (2014) 4491–4496.
- [22] H.K. Makadia, S.J. Siegel, Poly(lactic-co-glycolic acid) (PLGA) as biodegradable controlled drug delivery carrier, *Polymers* 3 (2011) 1377–1397.
- [23] R.A. Jain, The manufacturing techniques of various drug loaded biodegradable poly(lactide-co-glycolide) (PLGA) devices, *Biomaterials* 21 (2000) 2475–2490.
- [24] Q. Cai, G. Shi, J. Bei, S. Wang, Enzymatic degradation behavior and mechanism of poly(lactide-co-glycolide) foams by trypsin, *Biomaterials* 24 (2003) 629–638.
- [25] S.D. Allison, Effect of structural relaxation on the preparation and drug release behavior of poly(lactic-co-glycolic)acid microparticle drug delivery systems, *J. Pharm. Sci.* 97 (2008) 2022–2035.
- [26] M. Borden, M. Attawia, Y. Khan, C.T. Laurencin, Tissue engineered microsphere-based matrices for bone repair: design and evaluation, *Biomaterials* 23 (2002) 551–559.
- [27] D. Bendix, Chemical synthesis of polylactide and its copolymers for medical applications, *Polym. Degrad. Stab.* 59 (1998) 129–135.
- [28] P.B. Deasy, M. Finan, M.J. Meegan, Preparation and characterization of lactic/glycolic acid polymers and copolymers, *J. Microencapsul.* 6 (1989) 369–378.
- [29] C. Jerome, P. Lecomte, Recent advances in the synthesis of aliphatic polyesters by ring-opening polymerization, *Adv. Drug Deliv. Rev.* 60 (2008) 1056–1076.
- [30] V. Ntziachristos, Fluorescence molecular imaging, *Annu. Rev. Biomed. Eng.* 8 (2006) 1–33.
- [31] W. Kasprzyk, S. Bednarz, D. Bogdal, Luminescence phenomena of biodegradable photoluminescent poly(diol citrates), *Chem. Comm.* 49 (2013) 6445–6447.
- [32] J. Yang, D. Motlagh, J.B. Allen, A.R. Webb, M.R. Kibbe, O. Aalami, et al., Modulating expanded polytetrafluoroethylene vascular graft host response via citric acid-based biodegradable elastomers, *Adv. Mater.* 18 (2006) 1493–1498.
- [33] A.T.R. Williams, S.A. Winfield, J.N. Miller, Relative fluorescence quantum yield using a computer-controlled luminescence spectrometer, *Analyst* 108 (1983) 1067–1071.
- [34] J. Zhou, Y.T. Tsai, H. Weng, D.W. Baker, L. Tang, Real time monitoring of biomaterial-mediated inflammatory responses via macrophage-targeting NIR nanoprobes, *Biomaterials* 32 (2011) 9383–9390.
- [35] D. Wang, T. Imae, M. Miki, Fluorescence emission from PAMAM and PPI dendrimers, *J. Colloid Interface Sci.* 306 (2007) 222–227.
- [36] W. Yang, C.Y. Pan, Synthesis and fluorescent properties of biodegradable hyperbranched poly(amido amine)s, *Macromol. Rapid Commun.* 30 (2009) 2096–2101.
- [37] Data from online <<http://www.cincinnatichildrens.org/assets/0/78/1067/2481/2525/2527/d420beff-63a9-41d8-a18c-bbadea6693ac.pdf>>.